The Application of Flow Stress Model to Sheet Metal Forming Simulation

YI-KAI LIN, KANG-MING HSU and PING-KUN LEE

Iron & Steel Research & Development Department
China Steel Corporation

Flow Stress is the material characteristics required for the commercial finite element CAE codes to simulate material's hardening behavior during the metal forming process. Commercial stamping CAE codes accept various models for flow stress input. An accurate analysis must be based on an appropriate flow stress modeling. Three different models of flow stress were discussed in this study: the real Point listing of tensile test data, the Swift fitting curve, and Point listing plus Hollomon fitting curve. To investigate the effect of flow stress model on the analysis results, they were examined by conducting hemisphere forming simulations using a commercial CAE code, Pamstamp. Real hemisphere forming of 270MPa mild steel and advanced high strength steels of DP780 and DP980 were also conducted to verify the CAE analysis results and the steel grade effects.

1. INTRODUCTION

With the rapid development of the computer technology, the 3D finite element CAE (Compute-aided engineering) code (FEM) has been widely used to predict and to evaluate the complicated deformation of the metal forming process. Because it involves nonlinear and large material deformation, the application of an appropriate true stress-strain curve to the CAE code is important to exactly simulate the material hardening behavior during the forming process. Tensile test is the most common way to obtain the stress-strain curve. However, in tensile testing, the uniform extension usually ends when the maximum load is achieved. After that, the test specimen begins to neck and the state of stress is no more than uniaxial. Because the state of stress changes gradually from a simple uniaxial tension to a complicated condition of triaxial stress for a round bar or of biaxial stress for a thin strip, the tensile testing fails to determine the true uniaxial stress-strain once the necking starts. Therefore, for CAE applications in which the strain exceeds its value at the onset of necking, the tensile test cannot provide sufficient data for modeling. This can seriously limit the use of FEM for large strain simulations[1]. For this reason, several studies attempting to obtain the true stress-strain relation after the necking point have been proposed in the literature.

Kajberg et al.[2] proposed a method in which the material deformation process was captured with a digital camera and digital speckle photography (DSP) was used in plane pointwise displacement fields. The plastic strain is determined by numerical differentiation and assuming plastic incompressibility. By using inverse modeling, including finite element analyses (FEA) of the tension tests, the material parameters are adjusted to achieve a minimum in a so-called objective function based on the difference between the experimental and FE-calculated displacement and strain fields. Parsons et al.[3] used a CCD camera to acquire digitized images of the specimen surface at regular intervals during a tensile test, and the DIC (Digital image correlation) method was used to measure, in two dimensions, the local displacement gradient and the full field displacements during a standard uniaxial tension test. From the raw displacement data, the true stress–strain and volumetric strain behavior and full-field strain contours were constructed. Dan et al.[4] proposed a mesh-free PIM (Point interpolation mehtod) method to determine the stress- strain curve of larger-strain when plastic instability occurs in standard tension tests. Zhang et al.[5] proposed a method to determine the true stress-logarithmic strain relation from the load-thickness reduction curve of tensile specimens with rectangular cross-section. The method was initially developed for isotropic material and has been further modified for anisotropic materials[6].

This paper examines the effect of flow stress models on the finite element analysis results by conducting a hemisphere forming simulation using a Pamstamp CAE code. Three models of flow stress input were examined.

The models were the real point listing obtained from tensile test data up to the ultimate tensile strength, the Swift[7] fitting curve, and the point listing plus Hollomon[8] fitting curve. To verify the simulation results and the steel grade effects, real hemisphere forming of 270MPa mild steel and advanced high strength steels of DP780 and DP980 were also conducted.

2. MATERIAL CHARACTERISTICS

In this study, three different strength grades of the carbon steel, 270MPa, DP780MPa and DP980MPa were selected. In order to obtain the material flow stresses, tensile tests were conducted at room temperature using a universal testing machine. The engineering stresses and engineering strains were converted into true stresses and true strains up to the ultimate tensile strength by following two equations. The mechanical properties evaluated from the uniaxial tensile test are tabulated in Table 1.

$$\sigma = s\,(1+e) \quad \text{..... (1)}$$

$$\varepsilon = \ell n\,(1+e) \quad \text{..... (2)}$$

Where σ : true stress; ε : true strain; s : engineering stress; and e : engineering strain.

Modern finite element software often offers various models of flow stress input such as the Point list, the Hollomon law, and the Swift law (also called Swift-Krupkowsky law). Figure 1 shows an example of the flow stress models to input in the commercial CAE software, Pamstamp.

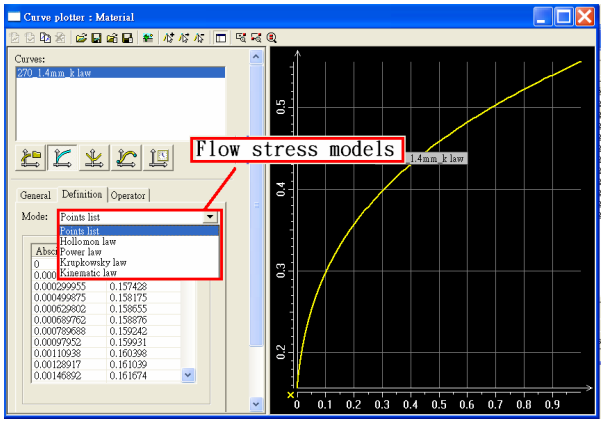

Fig. 1. Flow stress models offered in the Pamstamp.

Among the above models, the Point list model means two columns of true stress-strain data obtained from the tensile test up to the ultimate tensile strength. When the Point list is inputted to the CAE code, the default flow stress data beyond necking is regarded as a constant stress as shown in Fig. 2.

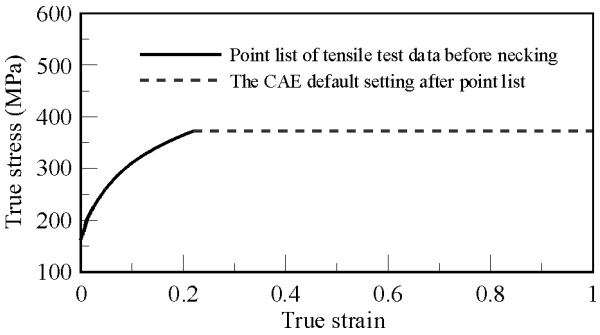

Fig. 2. Point list model in the CAE program.

In the model of Swift law, three material constants, strength coefficient (K), strain-hardening exponent (n) and initial strain (ε_0), should be estimated by curve fitting the measured true stress-strain data before necking to the following equation:

$$\sigma = K(\varepsilon_0 + \varepsilon)^n \quad \text{.....(3)}$$

For the model of the Hollomon law, two material constants, strength coefficient (K) and strain-hardening exponent (n), are estimated by curve fitting the measured true stress-strain data before necking to the following equation:

$$\sigma = K\,\varepsilon^n \quad \text{.....(4)}$$

Once the material constants of the Swift and Hollomon laws are obtained, the flow stress beyond the necking point can be extrapolated or predicted.

3. RESULTS AND DISCUSSION

3.1 Curve Fitting Results

Figure 3 shows the tensile test data of different steels fitted with the Hollomon and Swift laws. It is known that the curve fitted by the Swift law is quite

Table 1 Mechanical data evaluated from the uniaxial tensile tests

Sample Blank	Thickness (mm)	Yield strength (MPa)	Ultimate tensile strength(MPa)	Uniform Elongation (%)
270 Mild steel	1.4	163	299	25.2
DP 780 steel	1.4	466	825	12.3
DP 980 steel	1.4	643	1003	9.5

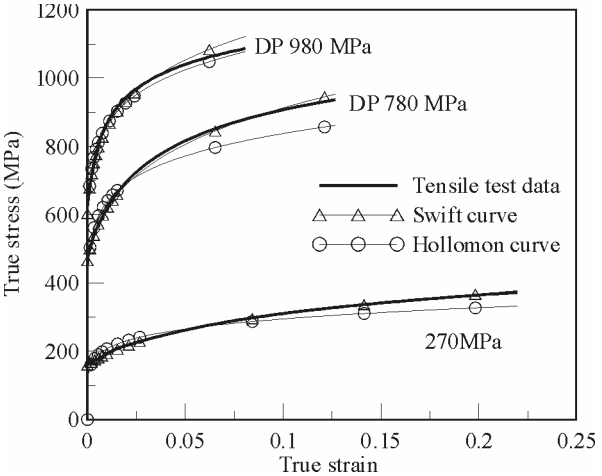

Fig. 3. Tensile test data of different steels fitted with the Hollomon and Swift laws.

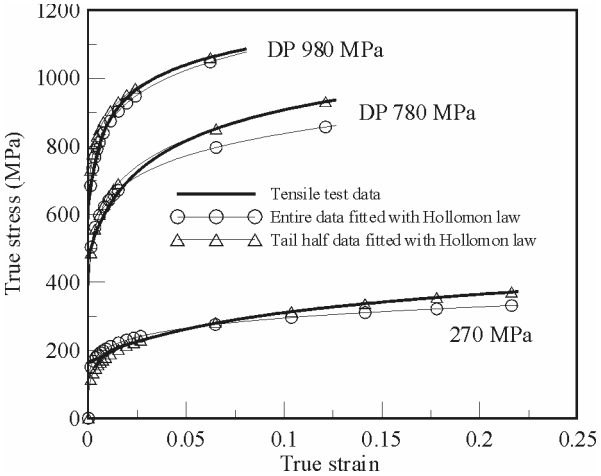

Fig. 4. Curves fitted with Hollomon law by using entire and tail half tensile test data.

coincident with the tensile test data for 270MPa mild steel. However, there is a discrepancy between the Swift curve and the experiment data for high strength steel. And this discrepancy increases with increasing steel strength grades, which means that the material characteristic of high strength steel may not be expressed by the Swift law very well. In addition, tensile test data is not best fitted with Hollomon law for all steels, compared with the Swift law. It seems that the initial stress or strain data will lower the fitting result by using the Hollomon law.

Figure 4 shows the Hollomon curve fitting results by using the entire and the tail half tensile test data respectively. It is obvious that the tail half data is better fitted with Hollomon law than the entire data for all steels. This indicates that the flow stress beyond the necking point may be well predicted by using the tail half data fitted with the Hollomon law. Therefore, this study will use the Point list plus Hollomon curve as one of the flow stress models for analysis.

The stress-strain relations for different steel strength grades obtained from different models are summarized in Table 2 and shown in Fig. 5. These flow stresses by different methods will be used in the finite element simulations of hemisphere forming in the next section. The simulation results of the thickness distribution will be compared with the real forming experimental results.

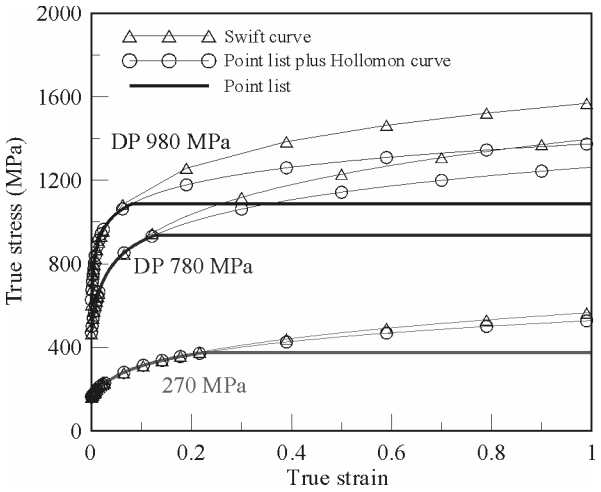

Fig. 5. Flow stresses for different steel strength grade obtained from different models.

3.2 Finite Element Modeling

An explicit dynamic finite element code "Pamstamp" was adopted to analyze the plastic deformation of the sheet blank in the hemisphere forming process. In the simulations, the tools are assumed to be rigid, and the blank is elastic-plastic. The flow stresses shown in Fig. 5 are adopted as the material parameters. The blank holder force is approximated to 100 kN. A constant friction coefficient is assumed at the interface between the blank and all tools. To obtain the real dynamic fric-

Table 2 Estimated parameters in the fitting equations (3) and (4) in this study

Fitting equation	Hollomon $\sigma = K\varepsilon^n$		Swift $\sigma = K(\varepsilon_0 + \varepsilon)^n$		
	K	n	K	ε_0	n
DP 980 MPa	1374.1	0.093	1569.92	0.0008	0.134
DP 780 MPa	1262.12	0.144	1396.92	0.0028	0.187
270 MPa	527.56	0.229	564.39	0.010	0.274

Table 3 Forming conditions for hemisphere forming simulation

Specimen	270 MPa	DP780 MPa	DP980 MPa
Bank thickness		1.4 mm	
Blank size		170mm×170mm	
Hemispherical punch		ϕ100mm	
Holding force		100KN	
Punch stroke		40 mm	
Friction coefficient	0.168	0.144	0.128

tion coefficient of the sample blanks, a flat sliding test (FST) was performed. The dynamic coefficient of friction for the three blanks is listed in Table 3. The blank of DP980 is a GA sheet. It possessed a lower value than the other two cold-rolled blanks. The configuration of the tools and blank before the hemisphere forming process is shown in Fig. 6. During the hemisphere forming simulation, the rectangular blank was clamped by the blank holder and die, and then the punch was moved down until the assigned stroke was reached. The forming conditions for the hemisphere forming simulation are listed in Table 3.

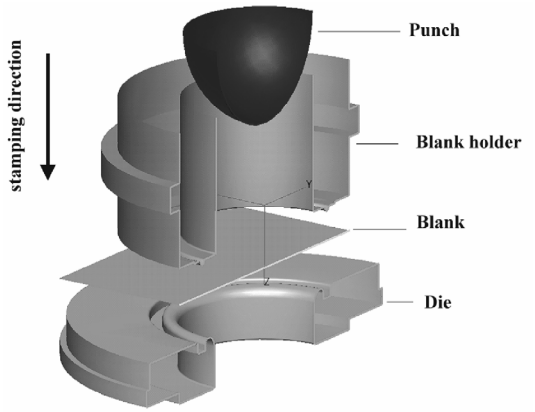

Fig. 6. Configuration of tools and blank before forming process.

3.3. Hemisphere Forming Experiment

To have a cross check with the simulation results, a real blank forming using a hemispherical punch of 100 mm in diameter was implemented. The experiment parameters are listed in Table 3. Three sample blanks of 270MPa mild steel, DP780, and DP980 were formed up to 40mm of punch stroke. Figure 7 shows the appearance of samples after forming. It was found that no significant drawbead formed in either of the blanks of DP780 and DP980, compared with that in blank of 270MPa. This suggests that the blanks of DP780 and DP980 are not completely held because a constant holding force of 100kN was applied to all blanks. The thickness distribution along the section A-A, as shown in Fig. 7 was measured to compare with the CAE simulation results.

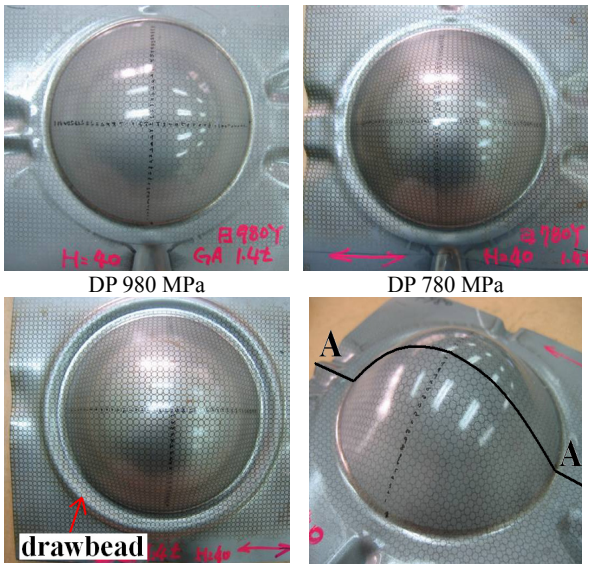

Fig. 7. Appearance of products after forming.

3.4 Compasison of Fem and Experiment

Figure 8 shows the simulation results of thickness distribution of 270MPa mild steel for different flow stress models and the real forming experiment result. It shows that the simulation results are in good agreement with the experiment. The Swift model (abbreviated as S model) and the Point list plus Hollomon model (abbreviated as P+H model) are relatively better than the Point list model (abbreviated as P model). There is a large deviation between the P model and the experiment at about ± (20 to 40) mm position, which may imply that the fitting of the flow stress curve beyond the necking point as a constant stress line is not adequate.

Figure 9 and Figure 10 show the CAE simulation and real forming experiment results of DP780 and DP980 respectively, and both steel grades have demonstrate similar results. It is known that the S model input is relatively closer to the experiment result than the others. The P model results of DP780 and DP980 have a large deviation at a large deformation as does that of 270MPa mild steel. This is resulted from the constant stress line of P model beyond necking. Therefore the P

model cannot express the material property completely. Comparing the result of 270 mild steel with that of high strength steel, it can be found that the deviation between the experiment and the S or P+H models became large for DP780 or DP980. This means that S or P+H models perhaps cannot predict the flow stress beyond the necking point very well for high strength steel. This will probably affect the accuracy for predicting springback.

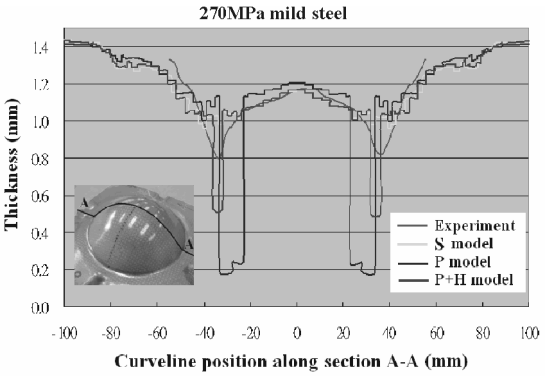

Fig. 8. Comparison of thickness distribution for 270 mild steel.

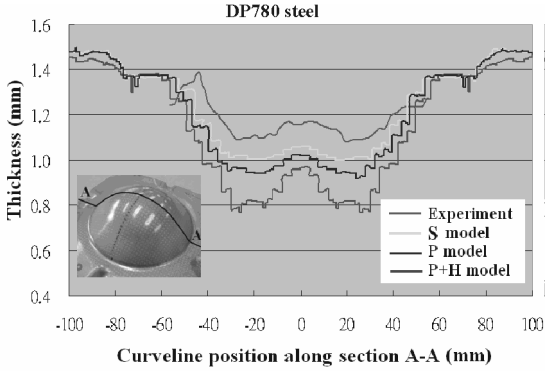

Fig. 9. Comparison of thickness distribution for DP 780 steel.

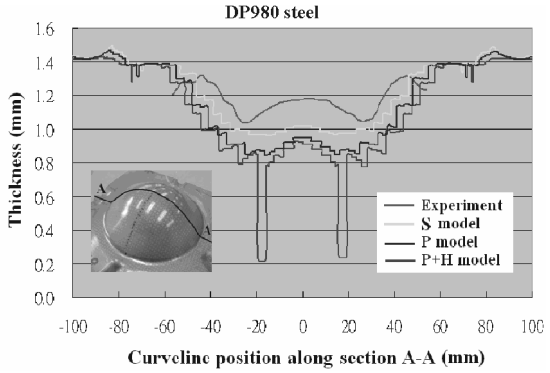

Fig. 10. Comparison of thickness distribution for DP 980 steel.

4. CONCLUSIONS

In this paper, the effect of flow stress models on a hemisphere forming simulation has been discussed. From comparison between the simulation and experiment results, the following conclusions can be drawn:

(1) The flow stress curve beyond the necking point should be predicted and inputted to the CAE software for good accuracy of simulations. The Swift model has relatively more accuracy than the Point list and the Point list plus Hollomon models for all steels.

(2) For the result of 270MPa mild steel, the Swift and Hollomon models do not affect the accuracy too much. That means that the CAE simulation is ripe and accurate for mild steel.

(3) The Swift or the Point list plus Hollomon models perhaps cannot predict the flow stress beyond necking point very well for advanced high strength steel. This will probably affect the accuracy of simulation for predicting springback. In current stage, however, these models are relatively better than the Point list model. They offer engineers a simple and quick choice in CAE simulation for advanced high strength steel.

REFERENCES

1. Y. Ling, "Uniaxial True Stress-Strain after Necking," AMP Journal of Technology, 1996, Vol.5, pp. 37-48.
2. J. Kajberg, G. Lindkvist, "Characterization of materials subjected to large strains by inverse modeling based on in-plane displacement fields," International Journal of Solids and Structures 41, 2004, pp. 3439-3459.
3. E. Parsons, M.C. Boyce, D.M. Parks, "An experimental investigation of the large-strain tensile behavior of neat and rubber-toughened polycarbonate," Polymer 45, 2004, pp. 2665-2684.
4. W.J. Dan, W.G. Zhang, S.H. Li, Z.Q. Lin, "A tensile characterization of metal sheet in large-strain," Proceedings of MSEC, 2006, pp. 1-8.
5. Z.L. Zhang, M. Hauge, J. Ødegard, C. Thaulow, "Determining material true stress-strain curve from tensile specimens with rectangular cross-section," International Journal of Solids and Structures 36, 1999, pp. 3497-3516.
6. Z.L. Zhang, J. Ødegard, O.P. Søvik, C. Thaulow, "A study on determining true stress–strain curve for anisotropic materials with rectangular tensile bars," International Journal of Solids and Structures 38, 2001, pp. 4489-4505.
7. J. Hollomon, "Tensile deformation," Transactions of the Society of Mining, Engineers of American Institute of Mining," Metallurgical and Petroleum Engineers, 1945, vol. 162, pp. 268-272.
8. H.W. Swift "Plastic Instability under Plane Stress," J Mech. Phys. Solids, 1952, vol. 1, pp. 1-18. □